The Journal of
Chemical Physics

RESEARCH ARTICLE | JUNE 09 2025

Chain conformations in adsorbed layer during polymer capillary imbibition

Tao Liang ; Li Peng ; Xianbo Huang; Jiajia Zhou

J. Chem. Phys. 162, 224901 (2025)
https://doi.org/10.1063/5.0270676

AIP Publishing

The Journal
of Chemical Physics

ARTICLE

pubs.aip.org/aip/jcp

Chain conformations in adsorbed layer during polymer capillary imbibition

Cite as: J. Chem. Phys. 162, 224901 (2025); doi: 10.1063/5.0270676
Submitted: 12 March 2025 • Accepted: 15 May 2025 •
Published Online: 9 June 2025

Tao Liang,[1,2] **Li Peng,**[3] **Xianbo Huang,**[3,a)] **and Jiajia Zhou**[1,2,b)]

AFFILIATIONS

[1] South China Advanced Institute for Soft Matter Science and Technology, School of Emergent Soft Matter,
South China University of Technology, Guangzhou 510640, China
[2] Guangdong Provincial Key Laboratory of Functional and Intelligent Hybrid Materials and Devices,
South China University of Technology, Guangzhou 510640, China
[3] National-Certified Enterprise Technology Center, Kingfa Science and Technology Co., LTD., Guangzhou 510663, China

[a)] huangxianbo@kingfa.com.cn
[b)] **Author to whom correspondence should be addressed:** zhouj2@scut.edu.cn

ABSTRACT

We conducted molecular dynamics simulations to investigate chain conformations in adsorbed layers during polymer capillary imbibition. While the imbibition length adheres to the classical Lucas–Washburn equation, a notable deviation in mobile bead density emerges under strong confinement, consistent with *in situ* dielectric spectroscopy experiments. The proportion of loop structures within adsorbed layers progressively increases during capillary infiltration, attributed to the relaxation of initially stretched chains toward equilibrium configurations. Furthermore, systematic analysis revealed that chain relaxation dynamics exhibit length-dependent retardation, especially under high confinement. The characteristic desorption time demonstrates chain-length dependence in quantitative agreement with scaling predictions.

I. INTRODUCTION

Understanding the capillary infiltration of polymers is important in many aspects, including nanotechnology,[1–3] separation of biomacromolecules,[4] and lab-on-chip device.[5] The capillary filling of simple liquids can be well described by the classic Lucas–Washburn equation (LWE),[6,7]

$$h(t) = \sqrt{\frac{\gamma R \cos\theta}{2\eta}}\, t^{1/2}, \qquad (1)$$

where $h(t)$ is the time-dependent infiltration length; R is the radius of the capillary tube; and γ, θ, and η are the surface tension, contact angle, and viscosity of the fluid, respectively.

A basic assumption of LWE is that the size of fluid particles is much less than the capillary radius; thus, the fluid can be treated as a continuous medium. This assumption is valid for simple fluids, for example, water (size 10^{-10} m) filling into mm-size glass tubes. However, when it comes to the infiltration of polymer melt ($R_g \approx 10$–100 nm) into self-ordered nanoporous aluminum oxide (AAO) (also $R = 10$–100 nm), there are noticeable deviations from the LWE prediction. The infiltration length $h(t)$ still follows the $t^{1/2}$ dependence, but the prefactor varies depending on the ratio between the polymer chain size and the capillary tube radius. A recent experiment[8] has reported a reversal in the dynamics of capillary filling with polymer molecular weight. The polymer melt of short chains shows a smaller prefactor than the LWE equation, while the polymer melt of longer chains displays a larger prefactor. Later, Yao *et al.*[9] proposed a unified theory to explain the reversal by demonstrating two competing mechanisms. One is the adsorption of chains on the surface of the capillary tube, which creates a dead layer and reduces the effective tube radius, resulting in a higher effective viscosity. The other is the reptation of chains under confinement, which allows the melt to exhibit a lower effective viscosity due to the disentanglement. Using molecular dynamics simulations,[10] we have confirmed the underlying molecular pictures proposed in Ref. 9. Yao *et al.*[11] also found an enrichment of the short chains inside the nanopores and near the pore surface by exploring the capillary imbibition of binary blends consisting of short and long chains.

The reversal occurs not only in capillary tubes with well-defined geometry but also in irregular geometries, such as porous media created by nanoparticle packing. The infiltration of unentangled polymer melt into nanoparticle packing slows down as the ratio between the polymer chain size and the average pore size (confinement ratio) increases.[12–14] Meanwhile, the infiltration of entangled polymer melt into nanoparticle packing enhances as the confinement ratio increases.[15,16] In a more recent study, Heo *et al.*[17] demonstrated that adsorbed layers could play an important role in polymer capillary filling. They explored the infiltration dynamics of poly(styrene-*stat*-2-vinyl-pyridine) (PS-*stat*-P2VP) statistical copolymers undergoing capillary filling into the interstices of silica nanoparticle packings (SiO_2 NP). They observed a non-monotonic dependence of the time required to fully fill SiO_2 NP on the fraction of 2VP. They ruled out the influence of other properties such as zero-shear viscosity and glass transition temperature and attributed the non-monotonic dependence to the adsorbed layers. The above results have shown that the adsorption of polymer chains on nanopore surfaces warrants deeper investigation.

Previously, the imbibition length was monitored by *ex situ* reflection microscopy,[8] which is time-consuming and lacks molecular information. The so-called *nanofluid* has been widely applied in the investigations of polymer properties under confinement.[18–21] In this method, two surfaces of AAO templates perpendicular to the infiltration direction are sputtered with a thin gold layer. This operation transforms the AAO templates to capacitors when an AC field is applied along the pore axes, and the dielectric signals are collected. Because the dielectric strength of the segmental process is proportional to the number density of dipoles, Tu *et al.* found that the dielectric strength increases linearly with the square root of time by the *in situ* monitoring time-dependent imbibition length $h(t)$ of PnBMA in nanopores.[22] For a different polymer *cis*-1,4-polyisoprene (*cis*-PI), which has a stronger interaction with the AAO surface than PnBMA did, the result is quite different.[23] In large and small nanopores, the dielectric strength of the segmental process increases linearly with the square root of time initially. However, it slows down for large nanopores and even kept constant for small nanopores at later times. Tu *et al.* constructed a plausible microscopic scenario to explain the experiment results.[23] In early stage of capillary filling, relative fewer chains are adsorbed on the surface of the capillary tube, and the adsorbed chains contain a small fraction of loop structures. However, in a later stage, more chains are adsorbed and the adsorbed chains contain a large fraction of loop structures. Chains that are not initially adsorbed on the surface become adsorbed onto the surface during the capillary filling process.

With *in situ* dielectric spectroscopy, Tu *et al.*[24] also measured the adsorption kinetics after full imbibition by following the evolution of the dielectrically active longest normal mode. The dielectric strength of the longest normal mode continues to decrease after full imbibition, which provides a way to characterize the adsorption kinetics of chains. The results show that adsorption characteristic time strongly depends on the ratio R_g/R. For a given pore radius, the molar dependence of characteristic adsorption time is in good agreement with a scaling theory developed by de Gennes.[25]

Previous studies have demonstrated the importance of adsorbed layers, but due to experimental difficulties, a comprehensive picture at molecular scale is still missing. In this work, we use molecular dynamics simulations to study the conformations of chains adsorbed on the tube surface. As the experimental results have shown, the chains on the capillary surface change conformation during and after capillary filling, and our simulation results provide a detailed analysis on this change. We have studied systems with different chain lengths and capillary tube radii, confirming the increment in the loop fraction of adsorbed chains and observing a stretched–relaxed transition of adsorbed chains.

This article is organized as follows: In Sec. II, we introduce the simulation model and some basic definitions, such as adsorbed repeat units, mobile repeat units, and the time of full infiltration. In Sec. III, we present the simulation results, including the conformations of adsorbed chains during capillary filling, the relaxation dynamics of chains, and the adsorption kinetics after full infiltration. Finally, in Sec. IV, we provide the summary of this article.

II. SIMULATION MODEL

We create a simulation box of size $40\sigma \times 40\sigma \times 200\sigma$ in x, y, z directions, as shown in Fig. 1(a), where the z-direction is parallel to the tube's axis. A single layer of face-centered cubic lattice beads (with a lattice constant of 2.467σ to prevent polymer melt from passing through), referred to as W, serves as a reservoir perpendicular to the z-axis at (0,0,0). Just above the center of the reservoir, we construct a cylindrical tube named T, along the z-axis. Cylindrical tubes with different capillary radii ($R = 5.85, 10.85, 15.85\sigma$) are formed by a single layer of square lattice beads, with a lattice spacing of 1.08σ. The tube height is set to $H = 70\sigma$. W beads within a capillary radius

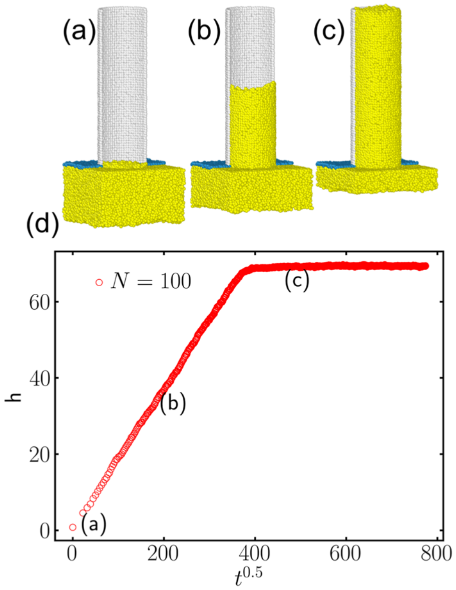

FIG. 1. Snapshots of our simulation model of the overall infiltration processes in system with radius $R = 10.85\sigma$ and chain length $N = 100$. [(a)–(c)] Snapshots corresponding to three time points that are labeled in (d). (d) Capillary infiltration height $h(t)$ as a function of $t^{0.5}$.

R are removed. All W and T beads are bonded to virtual beads at their initial position using a bond potential $U(r) = \frac{1}{2}kr^2$, where r is the bond length. This allows W and T beads to fluctuate around their initial positions, corresponding to the thermostat temperature.[10,26,27] The nonbonded potential between all beads is described by the truncated–shifted Lennard-Jones potential as Eq. (2) with a cutoff distance $r_{\text{cut}} = 2.5\sigma$ and $\sigma = 0.8$.[26] The strength of nonbonded interactions between W and T is set to be $\epsilon_{\text{TT}} = \epsilon_{\text{TW}} = \epsilon_{\text{WW}} = 1.0k_BT$, ensuring that polymer melt beads cannot pass through the W and T bead walls,

$$U(r) = \begin{cases} 4\epsilon_{\text{ij}}\left[\left(\frac{\sigma}{r}\right)^{12} - \left(\frac{\sigma}{r}\right)^{6} - \left(\frac{\sigma}{r_{\text{cut}}}\right)^{12} + \left(\frac{\sigma}{r_{\text{cut}}}\right)^{6}\right], & r \le r_{\text{cut}}, \\ 0, & r > r_{\text{cut}}. \end{cases} \tag{2}$$

We study five types of polymer chains named A with lengths $N = 50, 100, 200, 300, 400$. The bonded potential of polymer chains is described by the finite extension nonlinear elastic (FENE) potential,[28]

$$U_{\text{FENE}}(r) = -\frac{1}{2}k_{\text{spring}}R_{\text{max}}^2 \ln\left(1 - \frac{r^2}{R_{\text{max}}^2}\right), \tag{3}$$

where $k_{\text{spring}} = 30k_BT/\sigma^2$ and $R_{\text{max}} = 1.5\sigma$.

For capillary radii $R = 5.85\sigma$ and $R = 10.85\sigma$, the total number of polymer beads is 36 000, while for $R = 15.85\sigma$, it is 72 000. The strength of nonbonded interactions between polymer beads is set to $\epsilon_{\text{AA}} = 1.4k_BT$. Before capillary infiltration, we set the interaction strengths as $\epsilon_{\text{AW}} = 1.4k_BT$ and $\epsilon_{\text{AT}} = 0.5k_BT$ to allow the polymer melt to relax under the reservoir wall. After sufficient relaxation, we increase ϵ_{AT} from $0.5k_BT$ to $1.6k_BT$, initiating the infiltration process. We employ the dissipative particle dynamics thermostat,[29–31] with a temperature of $T = 1.0$ and a friction parameter of $\xi = 0.5$. The integration time step is set to $\Delta t = 0.005\tau$. Our simulations are conducted using the HOOMD-blue package.[32]

Since our goal is to study the chain conformations of the adsorbed layer, we first need to define the adsorbed layer. Previous studies[33–35] have shown that repeat units near planar surfaces exhibit a layered distribution, which can be characterized by the repeat unit density profile. The first layer of repeat units near an attractive substrate is typically considered the adsorbed layer. We calculate the repeat unit density profiles in systems with all three tube radii (as shown in Fig. S1), which all show a layered distribution. Based on this, we define repeat units within the first layer as adsorbed repeat units and chains containing at least one adsorbed repeat unit as adsorbed chains. Furthermore, we classify repeat units in all chains inside the tube into four types:

- **Train**: adsorbed repeat units in direct contact with the surface.
- **Loop**: non-adsorbed repeat unit sequences located between train segments.
- **Tail**: non-adsorbed repeat unit sequences at the ends of adsorbed chains.
- **Free**: chains with no repeat units in the adsorbed layers.

Because we need to analyze polymer chain conformations during and after capillary filling, we need to determine the time t^* of full infiltration. The imbibition length $h(t)$, as a linear function of square root of time $t^{1/2}$, is fitted by two trend lines: one during imbibition and the other after imbibition.[17] Then, the time t^* required to fully fill the capillary tube is determined by finding the intersection of two trend lines (the result is shown in Fig. S2).

III. RESULTS AND DISCUSSIONS

A. During capillary filling

As train structures are adsorbed on the capillary tube surface and the two ends of loop structures are fixed by train repeat units, they do not fluctuate over time and, therefore, make no contribution to the dielectric strength. To compare with the experimental results of dielectric strength, we define mobile repeat units as those that include tail structures in the adsorbed layers and free chains. We calculate the amount of mobile repeat units N_{mobile} during and after capillary infiltration. In the capillary filling of PnBMA, early experimental results[22] have shown that the dielectric strength $\Delta\epsilon(t)$ of the polymer melt inside the capillary tube increases linearly with $t^{1/2}$. However, in the capillary filling of *cis*-PI 42k,[23] the increase in dielectric strength slows down with a capillary tube radius of $R = 20$ nm (confinement ratio, $R_g/R = 0.35$). However, the slowing down phenomenon is less obvious with a capillary tube radius of $R = 50$ nm (confinement ratio, $R_g/R = 0.14$).

The amount of mobile repeat units N_{mobile} as a function of $t^{1/2}$ is shown in Fig. 2(a). In our simulation systems with tube radius $R = 5.85\sigma$, as the chain lengths range from $N = 50$ to $N = 400$, R_g/R ranges from 0.56 to 1.43. The confinement ratio (R_g/R) used in the simulations is comparable to that in the experiments. As the chain lengths increase, $N_{\text{mobile}}(t^{1/2})$ gradually shows two time regimes, with the second one being slower than the first one. The slowing down effect in the growth of mobile repeat units is more evident as the chain lengths increase. This can be explained by the increase in loop ratio and the decrease in tail ratio as the chain lengths increase (as shown in Fig. S3). However, it is difficult to identify the same tendency when capillary tube radii increase (the results are shown in Figs. S4 and S5). These results are consistent with experimental results[23] when the capillary tube is wider. When the radius of capillary tube increases, the ratio between surface and volume becomes smaller. The fraction of repeat units in adsorbed layers gradually decreases, so the adsorbed layers have less influence on the amount of mobile repeat units. Thus, the slowing down phenomenon is less obvious. The fraction of mobile repeat units among all repeat units inside the tube during the infiltration process with a capillary radius of $R = 5.85\sigma$ is shown in Fig. 2(b). The fractions of three kinds of chain lengths decrease during infiltration, which are consistent with the slowing down of N_{mobile}.

For polymer conformations in the adsorbed layers, we calculate the ratios of three types of repeat units (train, loop, and tail) during capillary infiltration. The result with a radius of $R = 5.85\sigma$ is shown in Fig. 3. In order to calculate the change in polymer conformations in early stages, we calculate the ratio of three types of repeat units when part of chain is inside the tube and adsorbed on the surface. Thus, we calculate the ratio of different types of repeat units $(f_{\text{train}}, f_{\text{loop}}, f_{\text{tail}})$ for the inner part of adsorbed chains. Figure 3 shows that, independent of chain length, f_{loop} increases in the early stage of capillary infiltration and f_{train} decreases simultaneously.

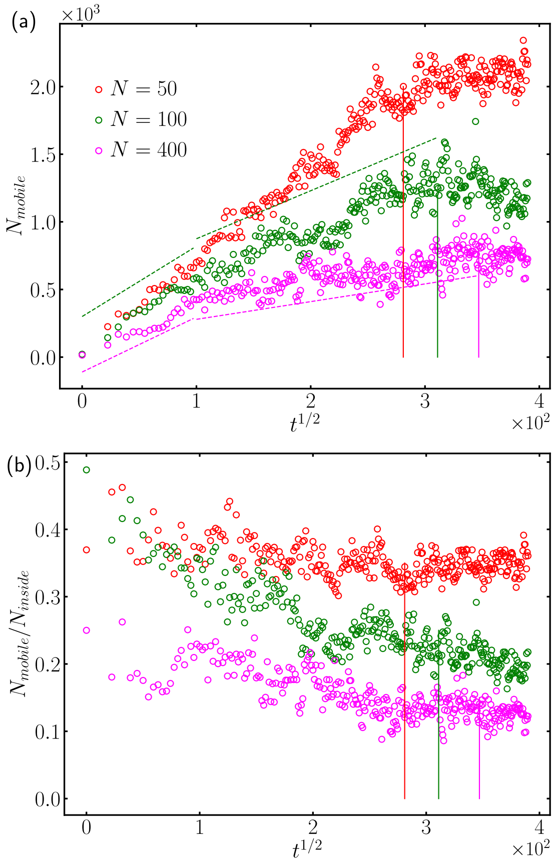

FIG. 2. The amount (a) and the fraction (b) of mobile repeat units vs $t^{1/2}$ with capillary radii $R = 5.85\sigma$; the polymer melt of length $N = 50$ is shown in red, $N = 100$ is shown in green, and $N = 400$ is shown in purple. The dashed lines show tendency at $t^{0.5} \in (0, 100)$ and $t^{0.5} \in (100, t^*)$. The vertical solid lines indicate the time t^* of full infiltration.

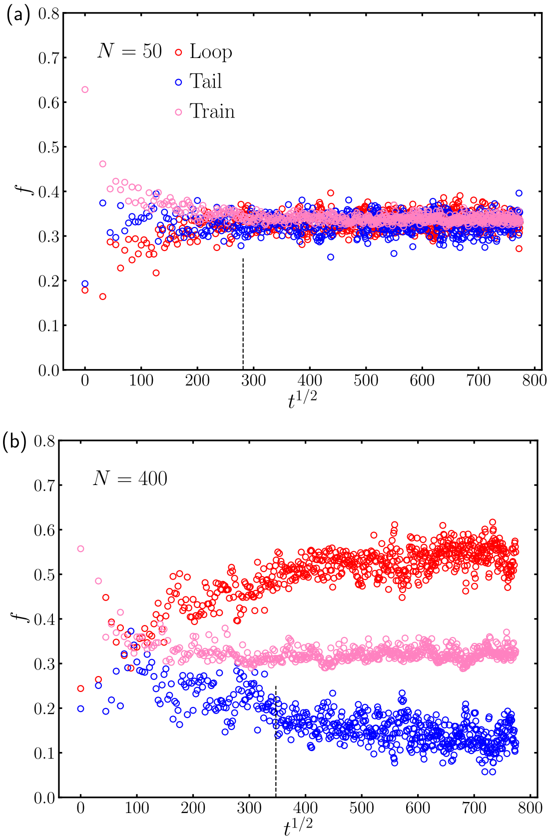

FIG. 3. Ratio of three types of structure of adsorbed monomers (loop shown in red, train shown in pink, and tail shown in blue) with capillary tube radii $R = 5.85\sigma$. (a) Chain length $N = 50$ and (b) chain length $N = 400$. The vertical dashed lines indicate the time when the capillary tube is fully filled.

For the tail type of monomers specifically, f_{tail} for chain length $N = 50$ almost remains constant during capillary filling while f_{tail} for chain length $N = 400$ gradually decreases simultaneously. In Fig. 4, tail lengths (L_{tail}) for both chain lengths $N = 50$ and $N = 400$ initially increase and then fluctuate around a constant value. We also calculate the length of chains that are both inside the tube, and some repeat units of the chain are adsorbed on the tube surface, denoted as L_{inside}. L_{inside} in a system of chain length $N = 50$ increases in the same way as the tail length. Therefore, the ratio of tail type of repeat units remains constant. However, L_{inside} for chain length $N = 400$ continues increasing during capillary infiltration because it takes more time for the whole chain to get inside the tube, which can explain the decrease in f_{tail} for chain length $N = 400$. Thus, we can attribute the increase in f_{loop} to the decrease in f_{train}. This result can be observed in systems with all radii and chain lengths (as shown in Fig. S7), which turns out to be a universal phenomenon.

We calculate the ratio of adsorbed chains f_{ads} among all chains inside the tube in a system with radius $R = 10.85$. The result in Fig. 5 shows that f_{ads} increases with time. The experimental result in a spectrum of normal modes[24] has shown the narrowing of the distribution of relaxation times with time. The authors contribute the broader distribution at the earlier stages to chain adsorptions. The result in Fig. 5 is consistent with the experimental result.

Our simulation model can reproduce the experimental results, as shown by the amount of mobile repeat units. The slowing down of the increase in N_{mobile} in a system with capillary tube radius $R = 5.85\sigma$ is consistent with the slowing down of dielectric strength in capillary with $R = 20$ nm. During capillary filling, the increase in f_{loop} and f_{ads} can confirm the assumption developed by Tu *et al.*[23]

In order to look deeper into the conformations of adsorbed layers, we also measure the end-to-end distance R_{ee} of adsorbed chains in three directions (x, y, z) during capillary infiltration. Unlike the calculation of three types of repeat units, here we only consider chains that are entirely inside the tube and have at least one repeat unit adsorbed on the surface. Here, we present the results for systems with radius $R = 5.85\sigma$ and chain lengths $N = 50, 100$, as shown in Fig. 6. We can observe that R_z first increases and then decreases to a constant value. The initial increase in R_z is due to the low contact angle ($\cos\theta > 0.8$[10]) between the polymer melt and the capillary tube surface under the condition of $\epsilon_{AT} = 1.6 k_B T/\sigma$. This

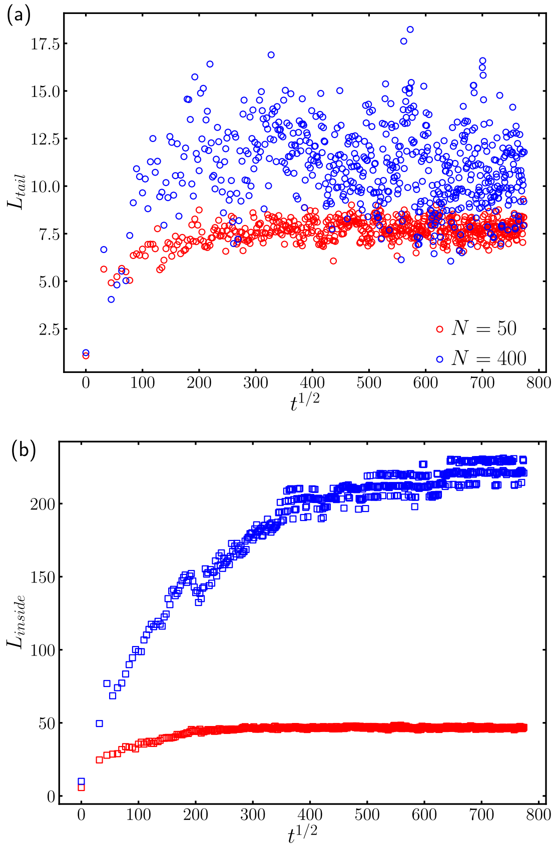

FIG. 4. (a) Average length of the tail structure of adsorbed chains L_{tail} during capillary infiltration. (b) Average length of part of adsorbed chains that are inside the capillary tube L_{inside} during capillary infiltration. Red: chain length $N = 50$; blue: chain length $N = 400$.

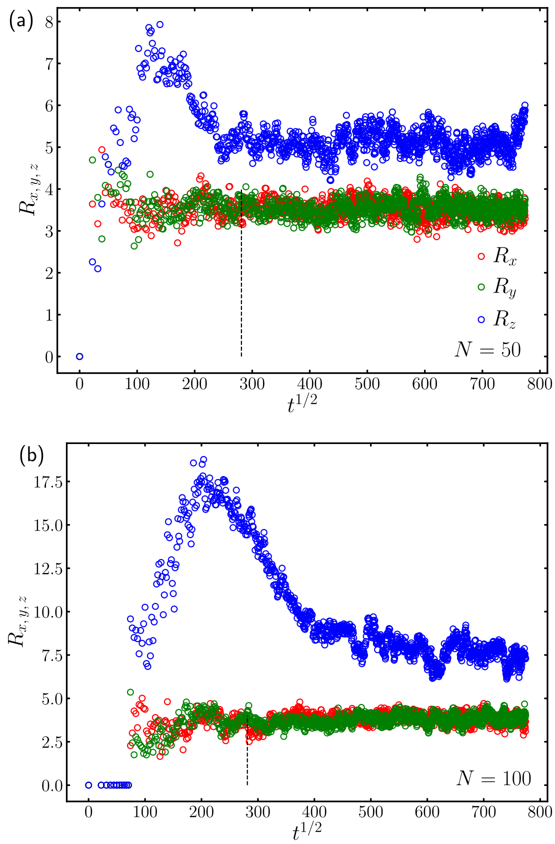

FIG. 6. End-to-end distances in x, y, z directions $R_{x,y,z}$ during capillary infiltration with tube radius $R = 5.85\sigma$. Chain lengths $N = 50$ (a) and $N = 100$ (b). The vertical dashed lines indicate the time when the capillary tube is fully filled.

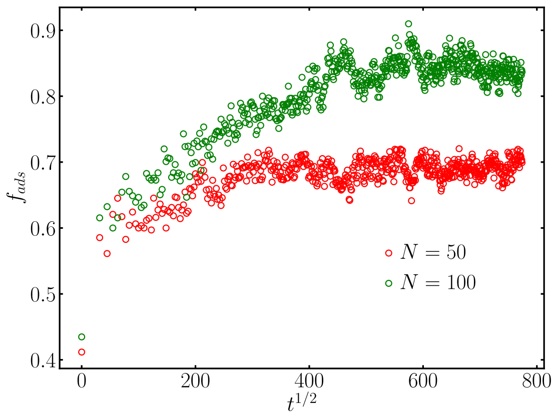

FIG. 5. Ratio between the amount of adsorbed chains and the amount of chains that are inside the tube in a system with tube radius $R = 10.85\sigma$ and chain length $N = 50, 100$.

phenomenon is similar to the adsorption of polymer onto a planar surface.[34,36–39] When chains initially adsorbed on a planar surface, they were stretched parallel onto the surface and then relaxed toward equilibrium states after fully adsorbed. These two different processes can explain the initial increase in R_z followed by its subsequent decrease. Both R_x and R_y remain constant during capillary infiltration, as the driving force acts along the z-direction. We also calculate the results in systems with radius $R = 5.85\sigma$ and longer chain lengths $N = 200, 300, 400$. It is difficult to observe the same phenomenon as it takes more time for chains to be entirely inside the tube (as shown in Fig. S8).

Based on these results, we propose one general picture of adsorbed chains during capillary infiltration. Initially, due to the relatively high velocity of the polymer melt, the adsorbed chains are rapidly stretched. As a result, more repeat units in the adsorbed chains are adsorbed on the surface, and the chains become highly oriented in the flow direction. As the velocity of polymer melt decreases, the adsorbed chains gradually relax toward their equilibrium states. Consequently, the loop structures increase and the adsorbed chains become less oriented, resembling the relaxation

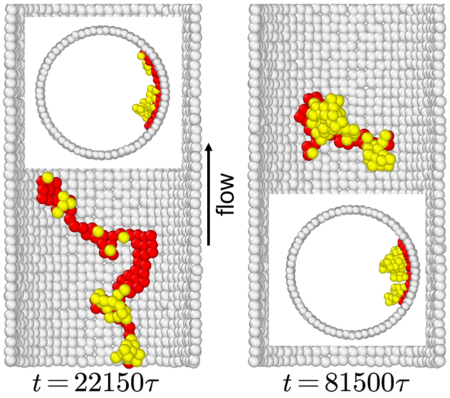

FIG. 7. Snapshot of one adsorbed chain at different times. The main and inset images show views along and perpendicular to the cylinder axis, respectively. Tube beads are shown in white, adsorbed beads are shown in red, and non-adsorbed beads (belonging to the adsorbed chain) are shown in yellow. The black arrow indicates the flow direction.

stage of chains adsorbed onto a planar surface. A snapshot of a system with chain length $N = 100$ and capillary radius $R = 10.85\sigma$ is shown in Fig. 7.

B. After capillary filling

After full infiltration, we explore the dynamic properties and adsorption kinetics of chains under confinement. First, we calculate the autocorrelation function of the end-to-end vector. The relaxation dynamics of chains inside the tube can be represented by autocorrelation functions, defined as follows:

$$C(t) = \frac{\langle R_t R_0 \rangle}{\langle |R_t \| R_0| \rangle}, \tag{4}$$

where R_t and R_0 are end-to-end vectors at a time interval t and $\langle \cdot \rangle$ represents the statistical average. Figure 8 shows the autocorrelation in system with a capillary tube radius of $R = 10.85\sigma$. The results indicate that the relaxation dynamics of chains slow down as the chain length increases. However, when the chain length is sufficiently long, the variation in dynamics becomes less pronounced, which can be attributed to the strong confinement of chains inside the tube. Under high confinement, chains are highly oriented along the tube axis, leading to extremely slow autocorrelation delay. Consequently, the differences in dynamics for longer chains become less obvious.

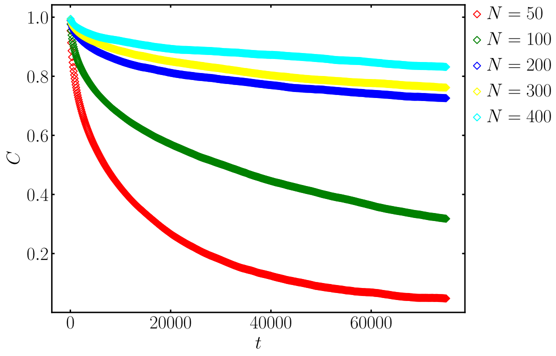

FIG. 8. Autocorrelation functions of the end-to-end vector in the system with tube radius $R = 10.85\sigma$.

The adsorption kinetics of repeat units and chains are investigated using the normalized survival functions of adsorbed repeat units and chains after full infiltration. At t^* when the capillary tube is fully filled, we label the adsorbed repeat units and the adsorbed chains. Their amounts are expressed as $N(0)$ and $n_c(0)$, respectively. After a time t since full infiltration, the amounts of the repeat units and chains that remain adsorbed are denoted as $N(t)$ and $n_c(t)$, respectively. The normalized survival functions of adsorbed repeat units $N(t)/N(0)$ and adsorbed chains $n_c(t)/n_c(0)$ can be fitted by a single exponential function,[40] defined as

$$N(t)/N(0) = \exp(-t/\tau_m), \tag{5}$$

$$n_c(t)/n_c(0) = \exp(-t/\tau_c), \tag{6}$$

where τ_m and τ_c are the characteristic adsorption times of repeat units and chains, respectively.

We analyze the chain length dependence of adsorption kinetics using systems with a constant tube radius and different chain lengths. Figure 9 presents the results for a system with tube radius

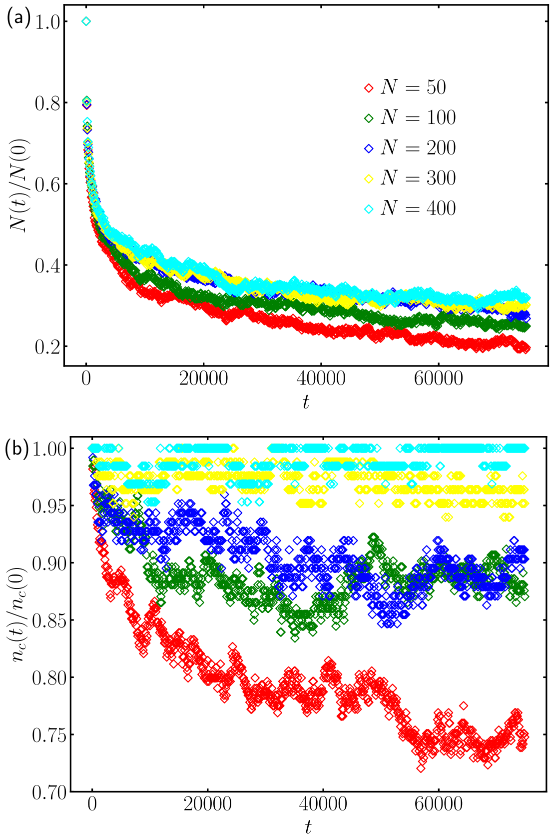

FIG. 9. Normalized adsorption survival functions of adsorbed repeat units (a) and adsorbed chains (b) after full infiltration in a system with tube radius $R = 10.85\sigma$.

$R = 10.85\sigma$. The survival function of repeat units indicates that repeat unit adsorption is a fast process and weakly depends on chain length, whereas chain adsorption is a slower process and strongly depends on chain length.

Figure 10(a) shows the result of adsorption characteristic times. For the kinetic of exchange between adsorbed and non-adsorbed chains, the scaling theory developed by de Gennes predicts the longest characteristic time scales as $\tau_c \sim \tau_m N^3$ when considering entanglement, where τ_m is the desorption time of a repeat unit. In our study, since the chain length ranges from below to above the entanglement threshold $(N_e = 80)$,[41,42] we observe a crossover from $\tau_c \sim \tau_m N^{0.87}$ to $\tau_c \sim \tau_m N^{3.01}$, which is consistent with scaling theory.

To study the influence of confinement on adsorption kinetics, we study systems with a constant chain length and different tube radii, as shown in Fig. 10(b). The results show that the characteristic adsorption time is a function of the degree of confinement R_g/R, where R_g is the chain's gyration radius in bulk. Thus, the characteristic adsorption time increases as the degree of confinement increases, which is consistent with the experimental results of Tu *et al.*[24]

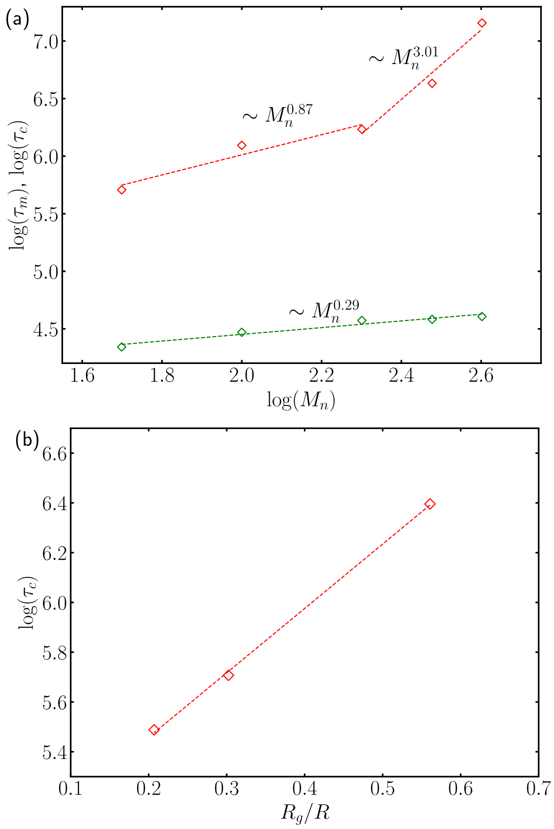

FIG. 10. (a) Chain length dependence of the desorption characteristic time for repeat units τ_m (green diamonds) and chains τ_c (red diamonds) after full infiltration. The dashed lines indicate linear fits. (b) Characteristic adsorption time of chains as a function of the degree of confinement, R_g/R.

IV. SUMMARY

In the first part, we explore the configurations of adsorbed chains during capillary in systems with different capillary radii and chain lengths. First, we calculate the time-dependent amount of mobile repeat units inside the capillary tube during infiltration. In the system with a capillary tube radius of $R = 5.85\sigma$, the increase in mobile repeat units slows down and the fraction of mobile repeat units among all repeat units inside the tube decreases during infiltration. These results are consistent with the experimental findings of dielectric strength in AAO arrays with a diameter of $R = 20$ nm. In systems with capillary tube radii $R = 10.85, 15.85\sigma$, this slowing-down tendency is not observed, which aligns with the experimental results in AAO arrays with a diameter of $R = 50$ nm. Thus, our simulation model successfully reproduces the experimental findings. Second, we calculate the fractions of three structural components (train, loop, and tail) in adsorbed chains. We find that f_{loop} increases, while f_{train} decreases during capillary infiltration. In addition, the end-to-end distance of adsorbed chains in the flow direction initially increases and then decreases at later times. These results suggest that an increase in f_{loop} is a consequence of a stretched–relaxed transition during capillary filling.

In the second part, we analyze the dynamic properties and adsorption kinetics after full infiltration. The results of the autocorrelation function show that the relaxation dynamics of chains inside the capillary tube decrease as the chain length increases. When the chain length is sufficiently long, relaxation dynamics become extremely slow due to strong confinement inside the capillary tube. The adsorption kinetics of repeat units and chains are also investigated. The characteristic desorption time of repeat units exhibits a weak chain length dependence, while the characteristic desorption time of chains shows a strong chain length dependence. The scaling relationship between the characteristic adsorption time and the chain length is consistent with the scaling theory developed by de Gennes.[25] The result in a system with a constant chain length and different tube radii shows that the characteristic adsorption time increases as the degree of confinement increases.

One possible extension of our work is to understand the influence of the adsorbed chains' conformations on the capillary filling of polymers of different architectures. With systems of statistical copolymers,[17] non-monotonic speed of imbibition was observed when the fraction of one type of monomer changes. The diblock copolymer presented another interesting subject. A more comprehensive understanding of adsorbed chains, including their interactions with free chains and the influence of chain orientation,[43] could significantly enhance our understanding of the dynamics underlying capillary imbibition.

SUPPLEMENTARY MATERIAL

See the supplementary material for a detailed simulation model, result, and discussion.

ACKNOWLEDGMENTS

This research was supported by the National Key R & D Program of China (Grant No. 2022YFE0103800), the National Natural

Science Foundation of China (Grant No. 22373036), R & D Program of Guangzhou (Grant No. 2024D03J0007), and Kingfa Science and Technology Company. The computation of this work was made possible by the facilities of Information and Network Engineering and Research Center of SCUT.

AUTHOR DECLARATIONS

Conflict of Interest

The authors have no conflicts to disclose.

Author Contributions

Tao Liang: Data curation (equal); Investigation (equal); Methodology (equal); Writing – original draft (equal); Writing – review & editing (equal). **Li Peng**: Conceptualization (equal); Writing – review & editing (equal). **Xianbo Huang**: Conceptualization (equal); Supervision (equal); Writing – review & editing (equal). **Jiajia Zhou**: Conceptualization (equal); Project administration (equal); Supervision (equal); Writing – review & editing (equal).

DATA AVAILABILITY

The data that support the findings of this study are available from the corresponding author upon reasonable request.

REFERENCES

[1] E. B. Stukalin, L.-H. Cai, N. A. Kumar, L. Leibler, and M. Rubinstein, "Self-healing of unentangled polymer networks with reversible bonds," Macromolecules **46**, 7525–7541 (2013).

[2] H. M. van der Kooij, A. Susa, S. J. García, S. van der Zwaag, and J. Sprakel, "Imaging the molecular motions of autonomous repair in a self-healing polymer," Adv. Mater. **29**, 1701017 (2017).

[3] H. Wang, H. Liu, Z. Cao, W. Li, X. Huang, Y. Zhu, F. Ling, H. Xu, Q. Wu, Y. Peng, B. Yang, R. Zhang, O. Kessler, G. Huang, and J. Wu, "Room-temperature autonomous self-healing glassy polymers with hyperbranched structure," Proc. Natl. Acad. Sci. U. S. A. **117**, 11299–11305 (2020).

[4] R. Bakry, C. W. Huck, and G. K. Bonn, "Recent applications of organic monoliths in capillary liquid chromatographic separation of biomolecules," J. Chromatogr. Sci. **47**, 418–431 (2009).

[5] A. Olanrewaju, M. Beaugrand, M. Yafia, and D. Juncker, "Capillary microfluidics in microchannels: From microfluidic networks to capillaric circuits," Lab Chip **18**, 2323–2347 (2018).

[6] R. Lucas, "Ueber das zeitgesetz des kapillaren aufstiegs von flüssigkeiten," Kolloid-Z. **23**, 15–22 (1918).

[7] E. W. Washburn, "The dynamics of capillary flow," Phys. Rev. **17**, 273–283 (1921).

[8] Y. Yao, S. Alexandris, F. Henrich, G. Auernhammer, M. Steinhart, H.-J. Butt, and G. Floudas, "Complex dynamics of capillary imbibition of poly(ethylene oxide) melts in nanoporous alumina," J. Chem. Phys. **146**, 203320 (2017).

[9] Y. Yao, H.-J. Butt, G. Floudas, J. Zhou, and M. Doi, "Theory on capillary filling of polymer melts in nanopores," Macromol. Rapid Commun. **39**, 1800087 (2018).

[10] J. Zhang, J. Lei, W. Tian, G. Zhang, G. Floudas, and J. Zhou, "Capillary filling of polymer chains in nanopores," Macromolecules **56**, 2258–2267 (2023).

[11] Y. Yao, H.-J. Butt, J. Zhou, M. Doi, and G. Floudas, "Capillary imbibition of polymer mixtures in nanopores," Macromolecules **51**, 3059–3065 (2018).

[12] J. L. Hor, H. Wang, Z. Fakhraai, and D. Lee, "Effect of physical nanoconfinement on the viscosity of unentangled polymers during capillary rise infiltration," Macromolecules **51**, 5069–5078 (2018).

[13] J. L. Hor, H. Wang, Z. Fakhraai, and D. Lee, "Effects of polymer–nanoparticle interactions on the viscosity of unentangled polymers under extreme nanoconfinement during capillary rise infiltration," Soft Matter **14**, 2438–2446 (2018).

[14] R. B. Venkatesh, N. Manohar, Y. Qiang, H. Wang, H. H. Tran, B. Q. Kim, A. Neuman, T. Ren, Z. Fakhraai, R. A. Riggleman, K. J. Stebe, K. Turner, and D. Lee, "Polymer-infiltrated nanoparticle films using capillarity-based techniques: Toward multifunctional coatings and membranes," Annu. Rev. Chem. Biomol. Eng. **12**, 411–437 (2021).

[15] R. B. Venkatesh and D. Lee, "Interfacial friction controls the motion of confined polymers in the pores of nanoparticle packings," Macromolecules **55**, 8659–8667 (2022).

[16] R. B. Venkatesh and D. Lee, "Conflicting effects of extreme nanoconfinement on the translational and segmental motion of entangled polymers," Macromolecules **55**, 4492–4501 (2022).

[17] T.-Y. Heo, T. Ienn, J. Bernard, R. A. Riggleman, and D. Lee, "Nonmonotonic impact of statistical copolymer composition on the kinetics of capillary rise infiltration," Macromolecules **57**, 10083–10090 (2024).

[18] A. Serghei, W. Zhao, X. Wei, D. Chen, and T. P. Russell, "Nanofluidics with phase separated block-copolymers: Glassy dynamics during capillary flow," Eur. Phys. J. Spec. Top. **189**, 95–101 (2010).

[19] A. Serghei, J. L. Lutkenhaus, D. F. Miranda, K. McEnnis, F. Kremer, and T. P. Russell, "Density fluctuations and phase transitions of ferroelectric polymer nanowires," Small **6**, 1822–1826 (2010).

[20] A. Serghei, D. Chen, D. H. Lee, and T. P. Russell, "Segmental dynamics of polymers during capillary flow into nanopores," Soft Matter **6**, 1111 (2010).

[21] A. Serghei, W. Zhao, D. Miranda, and T. P. Russell, "Curie transitions for attograms of ferroelectric polymers," Nano Lett. **13**, 577–580 (2013).

[22] C.-H. Tu, M. Steinhart, H.-J. Butt, and G. Floudas, "In situ monitoring of the imbibition of poly(n-butyl methacrylates) in nanoporous alumina by dielectric spectroscopy," Macromolecules **52**, 8167–8176 (2019).

[23] C.-H. Tu, J. Zhou, M. Doi, H.-J. Butt, and G. Floudas, "Interfacial interactions during *in situ* polymer imbibition in nanopores," Phys. Rev. Lett. **125**, 127802 (2020).

[24] C.-H. Tu, J. Zhou, H.-J. Butt, and G. Floudas, "Adsorption kinetics of cis-1,4-polyisoprene in nanopores by in situ nanodielectric spectroscopy," Macromolecules **54**, 6267–6274 (2021).

[25] P. G. de Gennes, "Polymers at an interface; a simplified view," Adv. Colloid Interface Sci. **27**, 189–209 (1987).

[26] D. I. Dimitrov, A. Milchev, and K. Binder, "Capillary rise in nanopores: Molecular dynamics evidence for the Lucas–Washburn equation," Phys. Rev. Lett. **99**, 054501 (2007).

[27] J. Zhang, J. Lei, P. Feng, G. Floudas, G. Zhang, and J. Zhou, "Capillary filling of star polymer melts in nanopores," J. Chem. Phys. **160**, 054903 (2024).

[28] K. Kremer and G. S. Grest, "Dynamics of entangled linear polymer melts: A molecular-dynamics simulation," J. Chem. Phys. **92**, 5057–5086 (1990).

[29] P. Español and P. Warren, "Statistical mechanics of dissipative particle dynamics," Europhys. Lett. **30**, 191–196 (1995).

[30] R. D. Groot and P. B. Warren, "Dissipative particle dynamics: Bridging the gap between atomistic and mesoscopic simulation," J. Chem. Phys. **107**, 4423–4435 (1997).

[31] C. Junghans, M. Praprotnik, and K. Kremer, "Transport properties controlled by a thermostat: An extended dissipative particle dynamics thermostat," Soft Matter **4**, 156–161 (2008).

[32] J. A. Anderson, J. Glaser, and S. C. Glotzer, "HOOMD-blue: A Python package for high-performance molecular dynamics and hard particle Monte Carlo simulations," Comput. Mater. Sci. **173**, 109363 (2020).

[33] K. A. Smith, M. Vladkov, and J.-L. Barrat, "Polymer melt near a solid surface: A molecular dynamics study of chain conformations and desorption dynamics," Macromolecules **38**, 571–580 (2004).

[34] A. De Virgiliis, A. Milchev, V. G. Rostiashvili, and T. A. Vilgis, "Structure and dynamics of a polymer melt at an attractive surface," Eur. Phys. J. E **35**, 97 (2012).

[35] Y. Zhou, J. Zhang, and J. Huang, "Dynamic propagation depth in substrate-supported polymer films: A molecular dynamics simulation," Macromolecules **56**, 2437–2446 (2023).

[36] P. Linse and N. Källrot, "Polymer adsorption from bulk solution onto planar surfaces: Effect of polymer flexibility and surface attraction in good solvent," Macromolecules **43**, 2054–2068 (2010).

[37] N. Källrot and P. Linse, "Dynamics of competitive polymer adsorption onto planar surfaces in good solvent," J. Phys. Chem. B **114**, 3741–3753 (2010).

[38] N. Källrot, M. Dahlqvist, and P. Linse, "Dynamics of polymer adsorption from bulk solution onto planar surfaces," Macromolecules **42**, 3641–3649 (2009).

[39] A. F. Behbahani, G. H. Motlagh, S. M. Vaez Allaei, and V. A. Harmandaris, "Structure and conformation of stereoregular poly(methyl methacrylate) chains adsorbed on graphene oxide and reduced graphene oxide via atomistic simulations," Macromolecules **52**, 3825–3838 (2019).

[40] J. F. Douglas, H. E. Johnson, and S. Granick, "A simple kinetic model of polymer adsorption and desorption," Science **262**, 2010–2012 (1993).

[41] R. Everaers, S. K. Sukumaran, G. S. Grest, C. Svaneborg, A. Sivasubramanian, and K. Kremer, "Rheology and microscopic topology of entangled polymeric liquids," Science **303**, 823–826 (2004).

[42] S. K. Sukumaran, G. S. Grest, K. Kremer, and R. Everaers, "Identifying the primitive path mesh in entangled polymer liquids," J. Polym. Sci., Part B: Polym. Phys. **43**, 917–933 (2005).

[43] S. Jeong, S. Cho, J. M. Kim, and C. Baig, "Molecular mechanisms of interfacial slip for polymer melts under shear flow," J. Rheol. **61**, 253–264 (2017).

Supplementary Information

Chain Conformations in Adsorbed Layer during Polymer Capillary Imbibition

1. SIMULATION MODEL

The density profiles of monomers as a function of distance r from the capillary tube axis with three radii $R = 5.85, 10.85, 15.85\,\sigma$ and chain length $N = 50$. The density profiles are drawn after full infiltration. As shown in Figure S1, monomers near inner surfaces exhibit a layered distribution. The valleys between the first two layers in three systems are all located in $R - 1.4\,\sigma$.

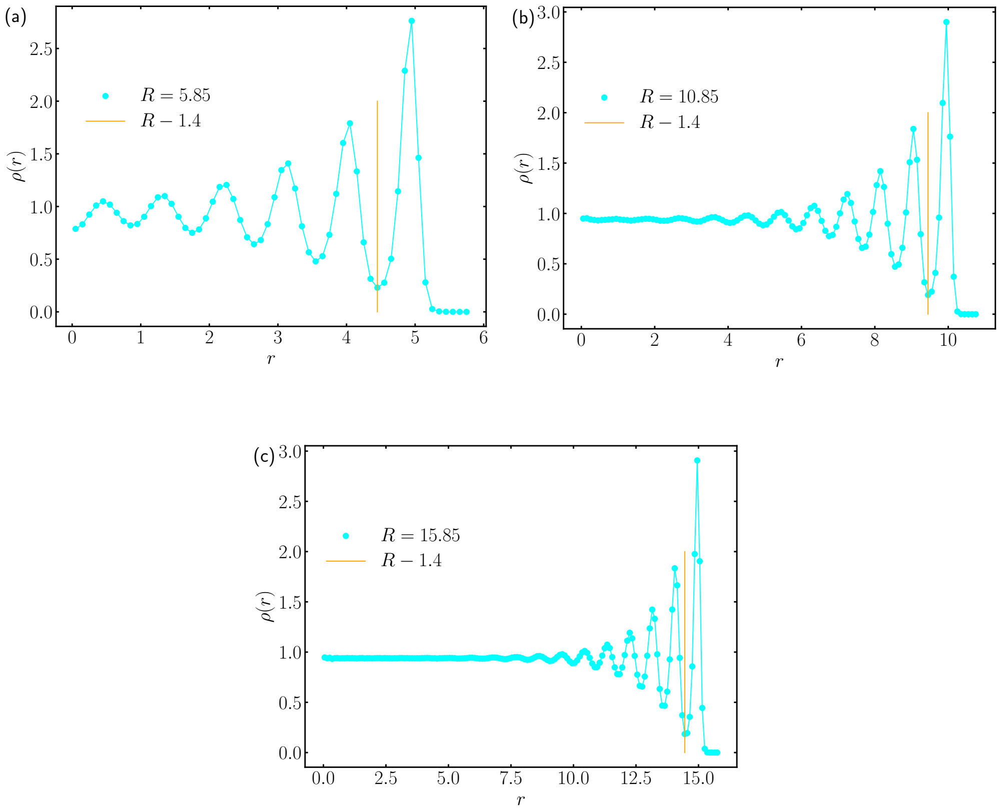

FIG. S1: The density profile of monomers as a function of distance r from the tube axis with radius $R = 5.85\,\sigma$ (a), $R = 10.85\,\sigma$ (b), $R = 15.85\,\sigma$ (c). The orange lines indicate the valleys between first two layers from surface.

Figure S2 shows the time-dependence of infiltration height $h(t)$ as a function of square root time. Two lines are fitted based on linear function from $h \in (40, 65)$ and $t^{0.5} > 500$, respectively. The intersection point of two lines indicates the time t^* when the capillary tube is fully filled.

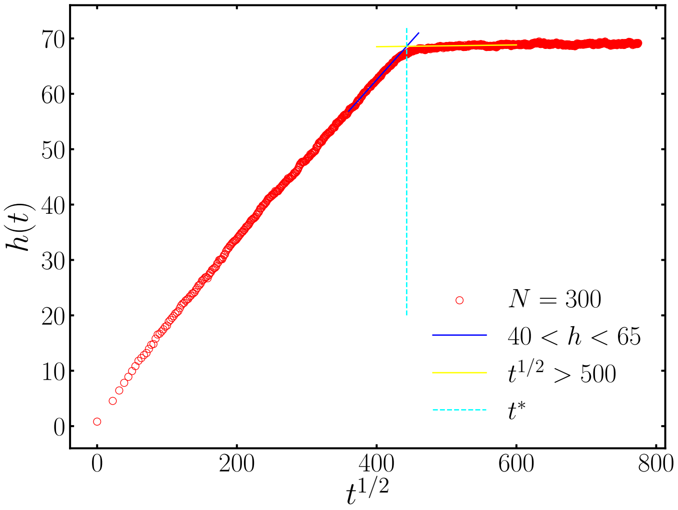

FIG. S2: The capillary infiltration height $h(t)$ as a function of $t^{1/2}$. Blue solid line is fitted based on linear function from $h \in (40, 65)$, yellow line is fitted from $t^{1/2} > 500$. Vertical cyan dash line locates at the intersection point of two solid lines.

2. RESULT AND DISCUSSION

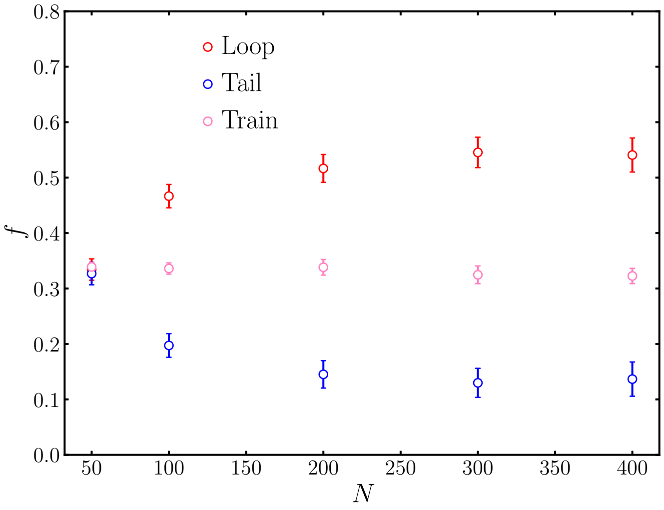

FIG. S3: The ratio of three kinds of repeat units in equilibrium state in system with tube radius $R = 5.85\,\sigma$ as chain lengths increase.

The fraction of mobile monomers among all monomers inside the capillary tube during infiltration process with capillary radius $R = 10.85\,\sigma$ is shown in Figure S4. The fraction of mobile monomers among all monomers inside the capillary tube with capillary radius $R = 15.85\,\sigma$ is shown in Figure S5.

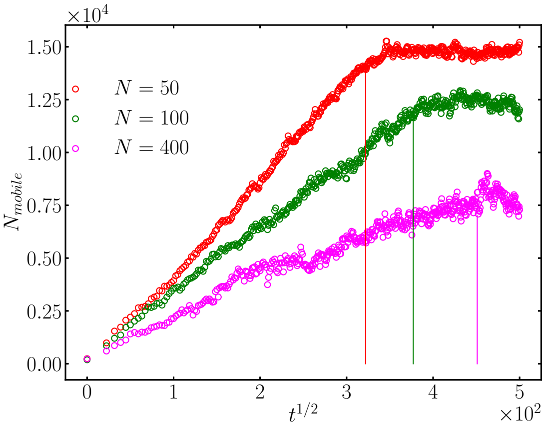

FIG. S4: The amount of mobile monomers versus $t^{1/2}$ with capillary radii $R = 10.85\sigma$, polymer melt of length $N = 50$ is shown in red, $N = 100$ is shown in green and $N = 400$ is shown in purple. The vertical solid lines indicate the time t^* when capillary is full filled.

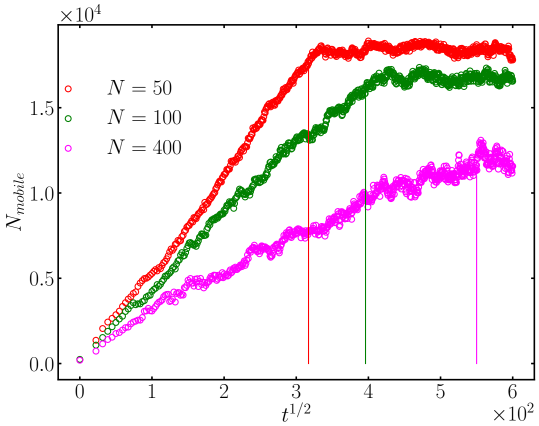

FIG. S5: The amount of mobile monomers versus $t^{1/2}$ with capillary radii $R = 15.85\sigma$, polymer melt of length $N = 50$ is shown in red, $N = 100$ is shown in green and $N = 400$ is shown in purple. The vertical solid lines indicate the time t^* when capillary is full filled.

We calculate the ratio f_{ads} between the amount of adsorbed chains and the amount of all chains inside the tube in system with tube radius $R = 10.85\,\sigma$ and chain lengths $N = 100$. The result in Figure S6 shows that f_{ads} increases with time. We label two time points which indicate two times when f_{ads} increase rapidly. Surprisingly, we can observe the decrease of f_{loop} in the same times in Figure S7. We could imagine that one free chain would contribute a large tail ratio and a small loop ratio if just one end gets adsorbed on the tube surface. That is why at the two labeled times, average loop ratio decrease and tail ratio increase.

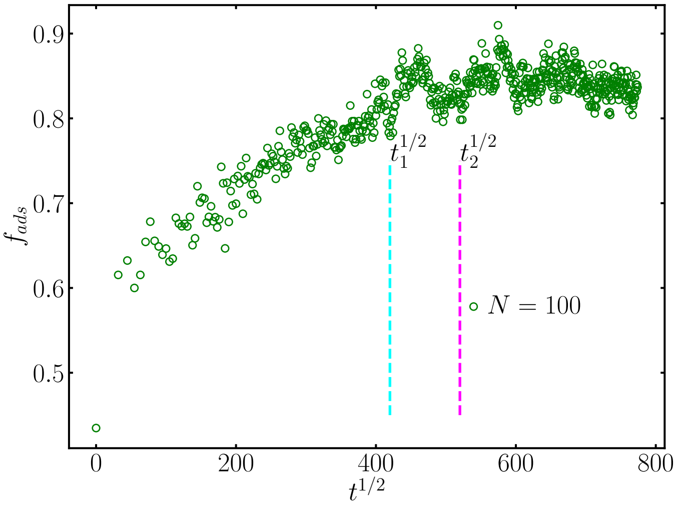

FIG. S6: The ratio between the amount of adsorbed chains and the amount of chains that are inside the tube in system with tube radius $R = 10.85\,\sigma$ and chain length $N = 100$. Two dashed lines indicate $t_1^{1/2} = 420$, $t_2^{1/2} = 520$, respectively.

The ratios of three types monomers of adsorbed chains in systems with all capillary radii $R = 5.85, 10.85, 15.85\,\sigma$ and all chain lengths $N = 50, 100, 200, 300, 400$ are shown in Figure S7. Although there are some differences, an increase in the ratio of loop monomers f_{loop} and a decrease in the ratio of train monomers f_{train} can be observed in all systems.

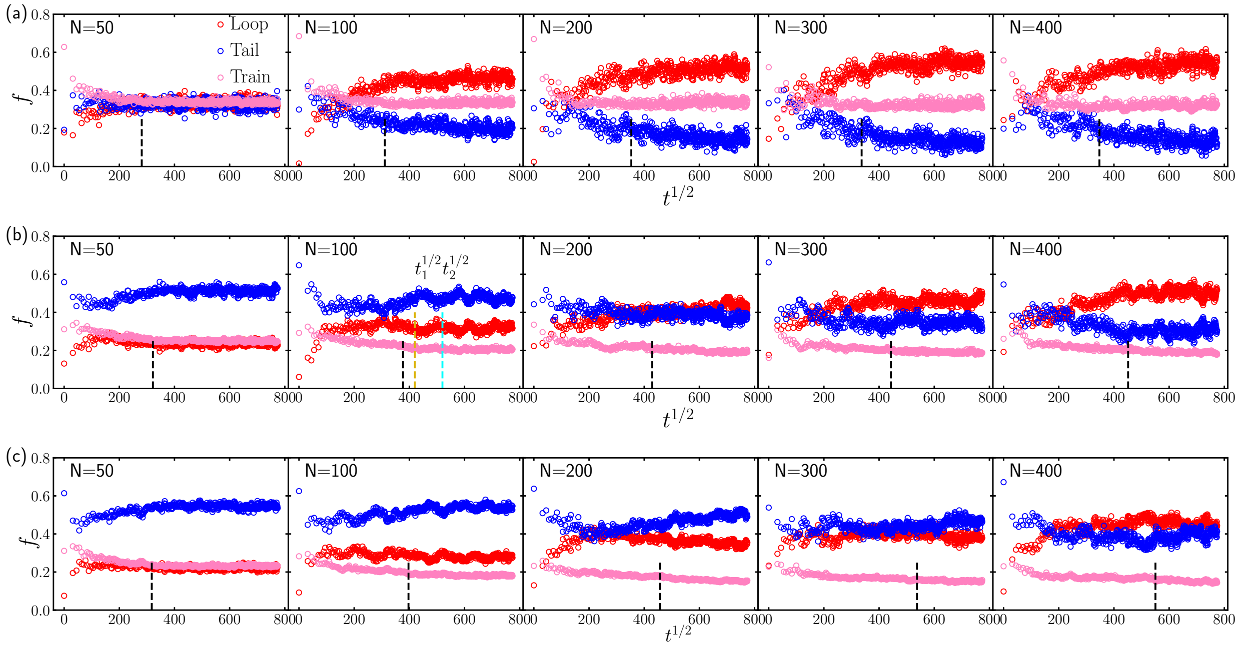

FIG. S7: The ratios of three types repeat units (loop shown in red, train shown in pink and tail shown in blue) in adsorbed layer with capillary tube radii $R = 5.85\sigma$ (a), $R = 10.85\sigma$ (b), $R = 15.85\sigma$ (c). The vertical black dashed lines indicate the time when capillary tube is fully filled. In system with $R = 10.85\,\sigma$ and $N = 100$, two colored dashed lines indicate $t_1^{1/2} = 420$, $t_2^{1/2} = 520$, respectively.

Figure S8 shows the results of end-to-end distances in (x, y, z) directions $R_{x,y,z}$ during capillary infiltration in systems with tube radius $R = 5.85\,\sigma$ and chain lengths $N = 200, 300, 400$.

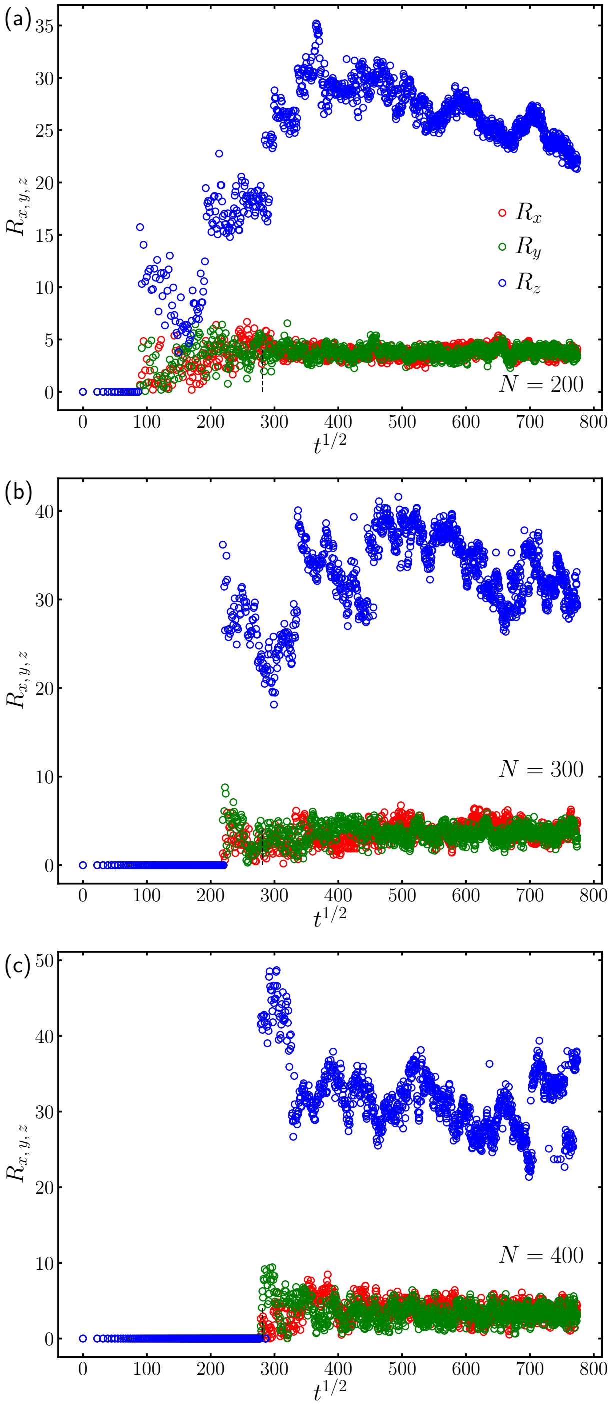

FIG. S8: The end-to-end distances in x, y, z directions $R_{x,y,z}$ during capillary infiltration with tube radius $R = 5.85\,\sigma$. Chain length $N = 200$ (a), $N = 300$ (b), $N = 400$ (c). The vertical dash lines indicate the time when capillary tube is fully filled.